



Analytical performance during ratiometric long-term imaging of pH in bioturbated sediments

Aron Hakonen^{a,*}, Stefan Hulth^a, Suzanne Dufour^b

^a Department of Chemistry, University of Gothenburg, SE-412 96 Göteborg, Sweden

^b Department of Earth and Planetary Sciences, McGill University, 3450 University Street, Montreal, QC, Canada

ARTICLE INFO

Article history:

Received 14 October 2009

Received in revised form 8 February 2010

Accepted 13 February 2010

Available online 20 February 2010

Keywords:

pH optode

Fluorescence imaging

Thyasira sarsi

Bioturbation

ABSTRACT

In this study, the long-term analytical performance of a high-resolution ratiometric imaging sensor for pH was quantitatively determined. The sensor was applied in an experimental microcosm to illustrate biogeochemical consequences from mining activities by the chemosymbiotic bivalve *Thyasira sarsi*. Utilizing time-correlated pixel-by-pixel calibration protocols during imaging, close to 90% of the pixels were associated with a precision (S.D.) of <0.05 pH units at the end of an experimental period of 17 days. For comparison, a precision of <0.05 pH units was achieved for less than 50% of the pixels throughout experiments using conventional pre-sample calibration procedures. The average standard deviation of pixels was 0.01 pH units. Image analysis of single pixel derivatives and pH measurements over time suggested that *T. sarsi* affect pH distributions and general sediment geochemistry more than would be expected based on the small size of the bivalves. A significant decrease of pH in the overlying water suggested a considerable release of reduced compounds from the exhalant stream of the thyasirids. Strong pH gradients were demonstrated not only across the sediment–water interface but, also associated with bioturbation activities immediately adjacent to *T. sarsi* burrowing tracts, inhalant tubes and pedal tracts in the sediment matrix. Gradients of up to 1.16 pH units per mm were observed.

© 2010 Elsevier B.V. All rights reserved.

1. Introduction

Optical sensors (optodes) have been found suitable for high-resolution imaging of gas and solute distributions in complex environments such as soil, aquatic sediments and living cells [1–6]. Typically, imaging optodes are made from a translucent thin polymer film or a sol–gel in which a solute sensitive fluorescent dye is immobilized by e.g. ionic interactions or covalent attachment [4,6–11]. After equilibration with the sample matrix (e.g. sediment pore water), the indicator film is illuminated and the light emitted from the sensor is collected on a CCD chip to obtain a two-dimensional image of solute distributions.

Analytical protocols for the normalization of artifacts and signal quality control are crucial in the design and use of intensity-based imaging optodes [12]. Although frequently used in a variety of applications, optical sensors are commonly susceptible to a drift in sensor response [7,8,12]. Sensor drift is a phenomenon only rarely acknowledged or fully compensated for by appropriate analytical protocols [12]. Several spectroscopic techniques and analytical calibration protocols, including the detection of luminescence by fluorescence lifetime and fluorescence ratiometry, are designed to normalize for signal drift and for sensor response not

associated with changes in analyte concentration [7,13–15]. The wavelength ratiometric normalization procedure is intended to efficiently remove artifacts in sensor response caused by e.g. variations in excitation light intensities, heterogeneous distribution of the indicator dye, photobleaching and leaching of the indicator dye [14,16]. For a ratiometric ammonium sensor, induced variations in oxygen concentrations, excitation light intensity and pH were more or less completely accounted for by the ratiometric procedure. It was, however, not possible to eliminate artifacts associated with fluctuations in temperature, effective indicator concentrations and sample ionic strength [17]. Fluorescence lifetime is a procedure often assumed insensitive to most analytical artifacts and therefore considered advantageous compared to, for example, the ratiometric approach. For a luminescent oxygen sensor, however, normalization by wavelength ratiometry improved the quality of measurements at least as much as sensing using fluorescence lifetime [15]. Stahl et al. [18] introduced an imaging sensor for pH based on time domain dual-lifetime referencing (t-DLR) into a sediment mesocosm. There was a continuous drift in the lifetime-ratiometric response (>0.1 pH unit) of this sensor during exposure to a phosphate buffer solution for 4 days. The authors presented an overall accuracy of ± 0.1 pH units and from the data a spatial resolution of ~ 0.1 pH unit could be calculated.

The time-correlated pixel-by-pixel calibration protocol, either utilizing linear or non-linear parameterization, provides a promis-

* Corresponding author. Fax: +46 31 772 13 94.

E-mail address: hakonen@chem.gu.se (A. Hakonen).

ing approach to further reduce artifacts during ratiometric fluorescence imaging with a unique set of calibrations for each pixel and time of measurement [8,12,19].

With increasing reports of low oxygen or anoxic conditions in coastal marine bottom waters world-wide [20,21], an appropriate understanding of the response of benthic communities to oxygen deficiency and organic enrichment is critical for remediation and a sustainable recovery of coastal ecosystems. For example, during re-colonization following eutrophication events, anoxic sediment layers may be re-oxidized through the irrigation and particle reworking activities (i.e. bioturbation) of early successional-stage benthic macrofauna [20]. In some habitats, early colonists include species that benefit from living near oxic/anoxic interfaces, such as invertebrates living in symbiosis with chemoautotrophic bacteria. Like other invertebrates bearing sulfide-oxidizing bacterial symbionts, the chemosymbiotic bivalve *Thyasira sarsi* requires access to both reduced sulfur and an energetically favorable oxidant for the successful maintenance of the symbionts on which they feed [22]. Irrigation and oxidation of burrows, cavities and sediment regions associated with *T. sarsi* pedal tracts may not only influence the community succession in *T. sarsi* habitats, but also affect the biogeochemistry and local cycling of redox sensitive elements such as iron and sulfur [23,24].

In this study, redox gradients as a direct result from organic matter mineralization, particle redistribution and irrigation by macrofauna were quantified by a high-resolution ratiometric imaging sensor for pH. The use of pH- instead of oxygen-imaging sensors was justified given the rapid consumption of oxygen introduced to anoxic sediments, which limits its detection over timescales larger than seconds. Biogeochemical consequences from oxygen within sediments and burrow constructions can, however, be inferred from ensuing chemically- or biologically-mediated redox reactions. Imaging studies have demonstrated that macrofaunal bioturbation may affect distributions of pH and CO₂ for several days [3,25]. While H⁺ is produced indirectly during microbial aerobic respiration, pH is directly affected in additional redox reactions that do not involve oxygen as an oxidant, or organic matter as a reductant. Examples include the diagenetic suite of reactions during organic matter mineralization (i.e. NO₃⁻-denitrification, Mn(IV)/Fe(III) and SO₄²⁻-reduction), as well as the reoxidation of NH₄⁺ (nitrification), Mn²⁺/Fe²⁺, and HS⁻ by oxygen or other oxidants [26,27]. Furthermore, oceanic uptake of anthropogenic CO₂ is presently altering the chemical signature of the world's oceans [28], with potential consequences for marine organisms, ecosystem functioning, and biogeochemical feedbacks, e.g. [29]. The majority of investigations on seawater acidification have focused on open water systems while; in contrast, benthic systems have only rarely been considered. The sensitivity and resilience of coastal benthic ecosystems towards a reduced pH in the overlying water are therefore virtually unknown.

The main objective of this study was to quantitatively evaluate the long-term analytical performance of a high-resolution ratiometric imaging sensor for pH, and to experimentally illustrate the versatility of imaging sensors in bioturbated sediments. To the best of our knowledge, there are no previous studies that include experimental data on the analytical performance of imaging sensors throughout experiments. Although Zhu et al. performed a 16-day study of pH distributions following macrofaunal reworking in marine sediments, no data on the analytical performance of the sensor during the experiment was presented [30].

Analytical procedures included ratiometric normalization of fluorescence and time-correlated pixel-by-pixel calibrations. Ecological implications of pH modifications in surface sediments as a consequence of *T. sarsi* activities are presented elsewhere (Dufour et al., manuscript).

2. Materials and procedures

2.1. General overview

Two adult specimens of *T. sarsi* were introduced to an experimental microcosm with sediment and overlying seawater, and net effects from faunal activities were periodically quantified by high-resolution imaging of pH distributions. There were 4 days between the collection of bivalves and the initiation of pH imaging. The sensor was applied into the experimental system and calibrated in the beginning and at the end of the experiment. Sensor operation lasted 17 days.

Bivalves and sediment were collected by an Olausson box-corer from the deepest part of the Gullmarsfjord (Alsback, 118 m), western Sweden. Surface sediment (~20 cm depth) was wet-sieved (1 mm grid) for use in the experimental microcosm. Retrieved specimens of *T. sarsi* (6–8 mm length) were kept in flow-through containers with unfiltered seawater (continuously supplied deep-water, 8°C) and sediment until their introduction to the microcosm 7 days later. The sampling site is exposed to seasonal cycles of bottom water oxygenation and organic matter deposition [31,32]. Due to high concentrations of Mn- and Fe-oxides in the solid phase of the sediment [33], sulfides are likely to be metal-bound. As a consequence, free sulfide is rarely released to the overlying bottom water despite periodically low oxygen concentrations. At this site, the organic content of the sediment is ~3% and the C/N ratio of the solid phase ~10 [33].

2.2. Experimental microcosm

The experimental microcosm (aquarium) was made in-house from two plates of transparent plexiglass (200 mm × 240 mm × 5 mm), separated by a silicone tube and fixed together by plastic screws and clamps. The aquarium was directly mounted on a PVC box containing the optical system (Fig. 1). The front wall of the microcosm could be quickly removed, providing easy access to the inner wall of the aquarium for sensor introduction and calibration. The inner width of the assembled aquarium was ~10 mm. On day 1, the aquarium was partially filled with a slurry of wet-sieved sediment which was allowed to settle for 2 days prior to the addition of two specimens of *T. sarsi*. During the course of experiment, a separate pump-system continuously supplied un-filtered, oxygenated deep-water from the Gullmarsfjord (Fig. 1). This water has a composition close to that of the sampling site. At the end of experiment, the microcosm was X-rayed (Andrex Smart, 300 kV, exposure 80 kV/1 mA, focal distance 60 cm, exposure time 4.5 min) to locate the thyasirids and their burrows. All experiments were performed in the dark in a temperature controlled (10°C) wet-laboratory.

2.3. Fluorosensor

The ratiometric imaging pH sensor was prepared according to [3]. In brief, a 15 cm × 20 cm sheet (100 μm polyester support, 10 μm cellulose acetate sensor layer) of transparent overhead film (HP C3835A) was immersed over night in filtered seawater with the pH sensitive ratiometric fluorophore 8-hydroxypyrene 1,3,6-trisulfonic acid (HPTS, 7.5 μM, >97%, Sigma Aldrich). The sensor was immersed in filtered seawater for 24 h prior to attachment to the inner wall of the microcosm. A black sheet of paper (120 μm thick) secured between the sensor foil and the sediment was used as optical isolation and mechanical protection. Total thickness of the immersed sensing layer and optical isolation was 200–300 μm due to the passive uptake of water during preconditioning.

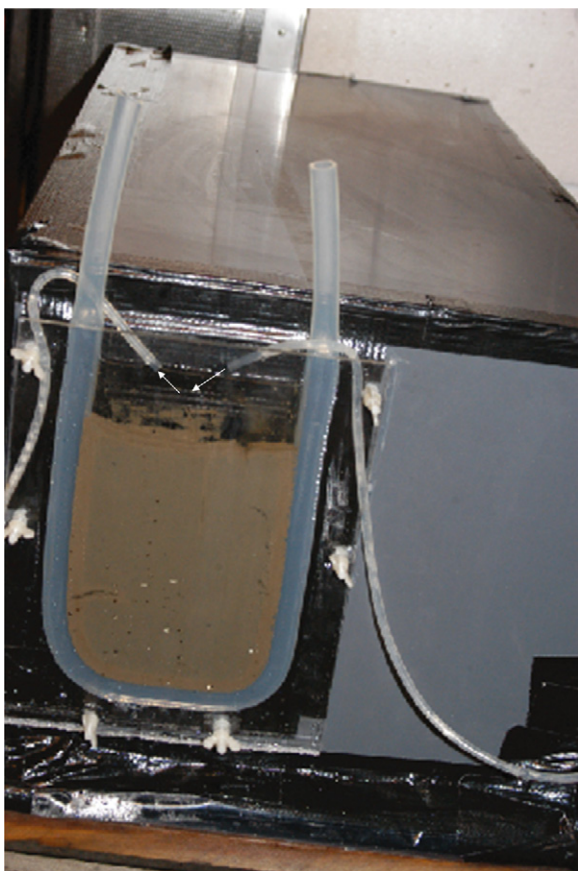


Fig. 1. The experimental microcosm (aquarium) was made from two plates of transparent plexiglass (200 mm × 240 mm × 5 mm), separated by a silicone tube. The inner width of the assembled aquarium was ~10 mm. The arrows indicate the in- and outflow of seawater. Observe that the inflow is directed to the left side of the aquarium which corresponds to the right-hand side of the optode images.

2.4. Optical setup

The optical system for imaging of pH included a 300 W xenon UV/VIS arc lamp with interchangeable band-pass filters (405 BP10 and 450 BP10 nm), a liquid light-guide, and a 16-bit CCD camera (Apogee Alta U13, 1280 × 1024 pixel resolution). A band-pass filter (510 BP10 nm) fixed between the Nikon standard SLR objective and the CCD chip provided appropriate emission wavelength. Pixels were binned 2 × 2, i.e. the effective pixel size was 277 μm × 277 μm. Sensor response 1–2 cm from the edge of the sensor was excluded from further treatment to minimize edge effects. Actual image size used for quantification was therefore 8.3 cm × 12.2 cm ($w \times h$, area ≈ 101 cm²). The dual excitation filter switch and the CCD camera were controlled by the software InCytIm2 and MaxImDL/CCD 4.51, respectively. The liquid light-guide, the CCD camera and the aquarium were fixed to an optical breadboard and enclosed within a dark-grey PVC box made in-house to minimize interferences from background light and to protect the CCD camera from the corrosive atmosphere in the wet-laboratory.

2.5. Sensor calibrations

The aquarium was filled with unfiltered seawater during the initial sensor calibrations performed prior to the addition of sediment and bivalves. Additions of 200 mM HCl sequentially adjusted pH of the seawater to 8.196, 7.981, 7.639, 7.393, 7.145, 7.011, 6.755 and 6.587. Five consecutive images of the fluorescence ratio ($R = F_1/F_2$) were acquired at each pH. A pH-electrode (model 6.0232.100, 780

pH meter; Metrohm Ltd.) was used to determine the pH (NIST) of the calibration solutions. At the end of experiment, the microcosm was dismantled, the sediment gently removed and the surface of the optical sensor carefully rinsed with seawater. The sensor calibration procedure was repeated at pH 8.170, 7.967, 7.679, 7.368, 7.190, 7.030, 6.862 and 6.715. Set of calibrations were linearly linked in time to provide a unique calibration in each pixel at each time of sampling [12].

2.6. Image acquisition and analysis

After adding the two bivalves, 68 images were acquired over a period of 8 days (day 3 to day 11) for long-term imaging of pH in bioturbated sediments. An additional 12 images were taken before ($n=6$) and after ($n=6$) the sediment was X-rayed at the end of experiments (day 17). During the course of experiments, images were primarily taken from 8 AM to 9 PM. Occasionally and in response to visual observations of faunal activities, images were acquired more frequently. The following image sequence was pre-set: (1) $F_{2,\text{dark}}$ ($\lambda_{\text{ex/em}}$: 450/510 nm, camera shutter closed); (2) $F_{2,\text{light}}$ ($\lambda_{\text{ex/em}}$: 450/510 nm); (3) $F_{1,\text{dark}}$ ($\lambda_{\text{ex/em}}$: 405/510 nm, camera shutter closed); (4) $F_{1,\text{light}}$ ($\lambda_{\text{ex/em}}$: 405/510 nm). Integration time was 10 s. For each excitation wavelength, the respective dark images with background noise were subtracted from images of fluorescence (i.e. $F_1 = F_{1,\text{light}} - F_{1,\text{dark}}$ and $F_2 = F_{2,\text{light}} - F_{2,\text{dark}}$). The ratiometric pH response ($R = F_1/F_2$) of the sensor was determined as the fluorescence ratio between F_1 ($\lambda_{\text{ex/em}}$: 405/510 nm) and F_2 ($\lambda_{\text{ex/em}}$: 450/510 nm) in each effective pixel after dark image correction.

Image analysis was performed using Matlab 6.5. By the time-correlated calibration procedure, obtained fluorescence ratio of images could be evaluated using a response function unique for each pixel, individually determined at the time of detection [12]. The pH in each pixel was median filtered (3 × 3 pixels) to remove salt and pepper noise while still preserving the edge response. Quiver plots were generated by the gradient (extracting partial derivatives) and quiver (vectorizing) functions in Matlab [2]. The partial derivatives were used to calculate the magnitude (M) of the gradient in each pixel ($M = [\delta x^2 + \delta y^2]^{1/2}$).

2.7. Analytical performance

For quality control and to compare between the time-correlated and more conventional calibration protocols, two different approaches were used to quantify the spatial and temporal precision of measurements. In the first approach, the spatial precision in a pixel was defined as the standard deviation (S.D.) of measurements in the 3 × 3 neighbouring group of pixels. This approach was motivated by the fact that pixel values have been extracted by median filtration (3 × 3 pixels), and that pixels do not have discrete optical pathways. The latter implies potential scattering of light within the sensor and divergence of light between the sensor and the optical set-up. Preliminary experiments with this particular optical system have shown that about 30% of the signal detected in a pixel can also be detected in the neighbouring pixels (data not shown). In the second approach, the temporal precision in a pixel was defined as the S.D. of the pixel response from six images acquired consecutively at the end of experiments (day 17). It was assumed that sensor response after about 17 days of experiments would provide the most unfavorable analytical precision throughout the experimental period.

To further evaluate sensor performance and to distinguish between systematic errors and bivalve activities, images captured during mornings and evenings were analyzed in blocks of 5 × 5 pixels (as in the quiver plots). Statistical significance related to an integrated pH response was thereby increased at the expense of

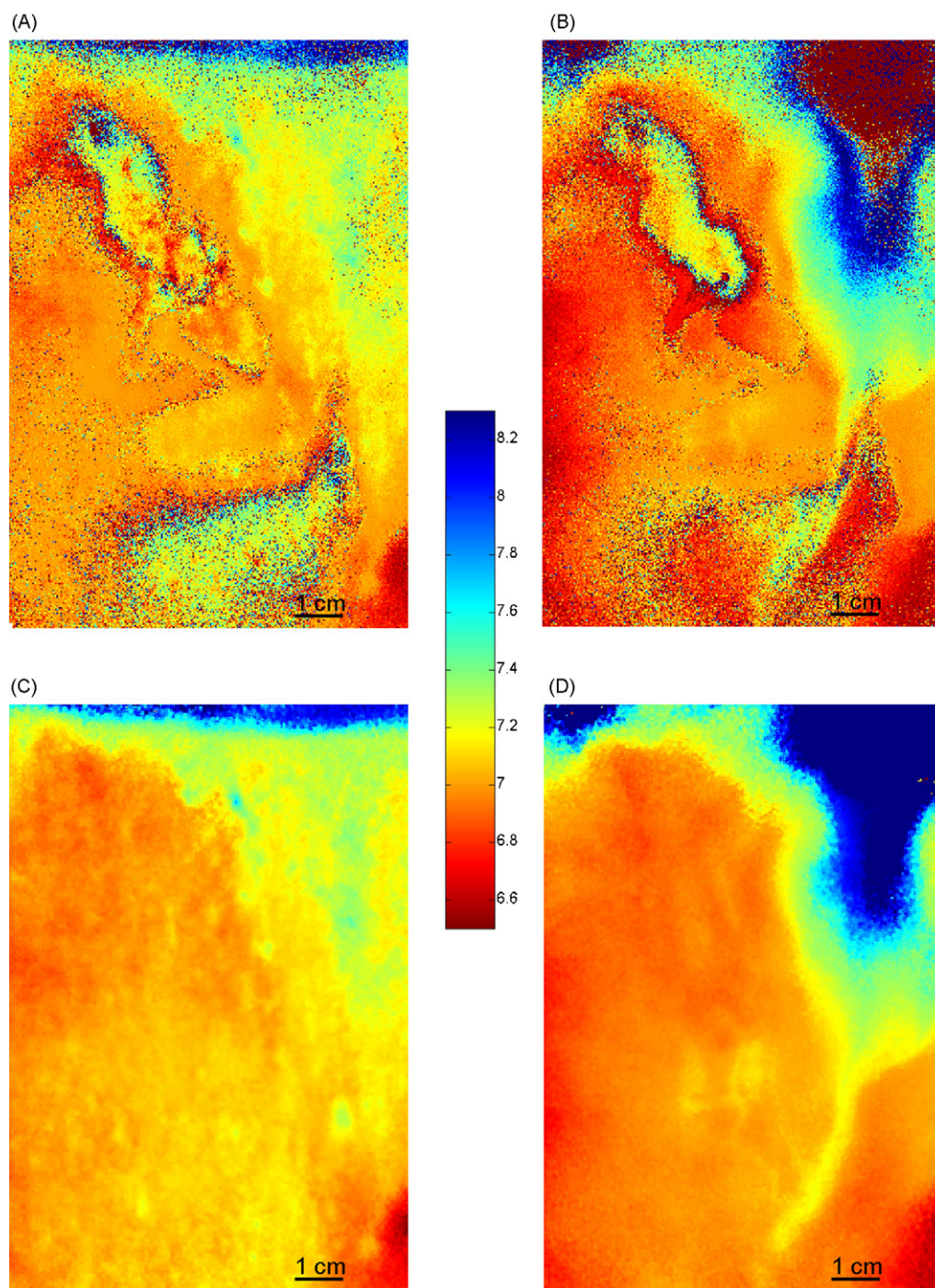


Fig. 2. Distribution of pH illustrated by ratiometric images without (A and B) and with (C and D) the time-correlated calibration protocol, here exemplified after 76 h (A and C) and 406 h (B and D) of experiment. Images A and B revealed areas of salt and pepper noise, while fine structures became evident after the normalization protocol (C and D). The colorbar displays pH values.

spatial resolution. Each group of blocked pixels for analysis corresponded to an area $<2 \text{ mm}^2$.

3. Results and discussion

3.1. Calibration assessment and analytical performance

Analytical developments to normalize fluorescence response and to compensate for signal drift over time include ratiometric sensing schemes coupled to time-correlated calibration procedures [12]. A comparison of ratiometric images with and without the

time-correlated calibration protocol indicated that uncorrected images have large areas of seemingly noisy response patterns (Fig. 2A and B), while even fine structures became evident after the normalization protocol was applied to images (e.g. Fig. 2D).

Overall, sensitivity and precision were reduced in regions with high pH (~ 8) due to the apparent pK_a (pK_a') of immobilized HPTS, $pK_a' \approx 6.4$ [3]. The dynamic range of optical sensors is normally considered to cover a pH range of $pK_a' \pm 1$ pH units [34]. Accordingly, imaging pH sensors based on HPTS (immobilized as in this study) have a theoretical maximum performance within the interval $5.4 \leq \text{pH} \leq 7.4$. Although pH of many subsurface marine

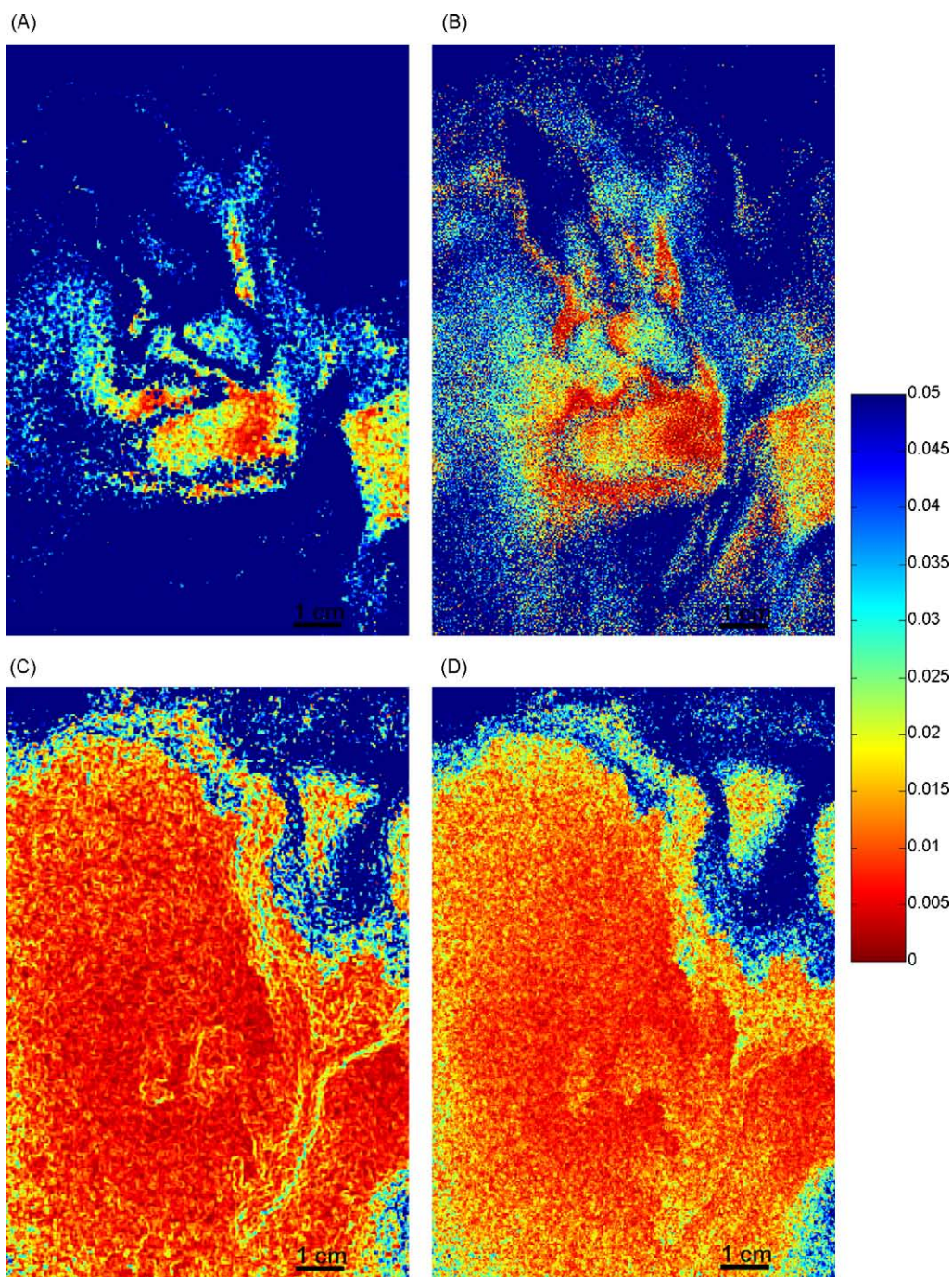


Fig. 3. Quantitative image of the analytical performance at the end of experiments (day 17) illustrated as the spatial (A and C, 3×3 group of pixels) and temporal (B and D, six consecutive images) precision of measurements (S.D.) in each pixel. Images A and B were evaluated using pre-sample calibration, while time-correlated protocols were applied to C and D. The colorbar displays S.D. of measurements (pH units).

sediments is ~ 7 [3,4], this range is somewhat below the pH often found in other marine systems [35]. However, optimal range of sensor performance is determined by how well low concentrations of indicator species can be detected [3]. For example, the dynamic range would cover 4 pH units ($\text{pK}_a' \pm 2$ pH units) if either of the two species in the indicator acid/base conjugate pair of HPTS could be measured at a relative concentration of 1%. Using modern optical technology, this is normally readily achieved. Further, from an analytical perspective it often is more appropriate to discuss analytical performance in a quantitative manner, for example in relation to a preset precision of measurements. The HPTS analogue, 6,8-dihydroxypyrene-1,3-disulfonic acid (DHPDS), was

recently immobilized in a sensor membrane for high-performance (e.g. precision 0.0057 pH units) measurements of pH between pH 6 and 9 [36]. This pH dye demonstrated a log-linear relationship with pH over 5 pH units. DHPDS may thus provide an interesting alternative to HPTS for pH measurements in marine environments, including pH distributions in sediments with a large range in pH.

The spatial precision of measurements was utilized to compare the analytical performance of the pH sensor throughout the experiment (all images), applying conventional calibration (pre-sample) and time-correlated-calibration protocols. During the first 10 days of experiment, >98% of pixels were associated with a precision better than 0.05 pH units using the time-correlated calibration pro-

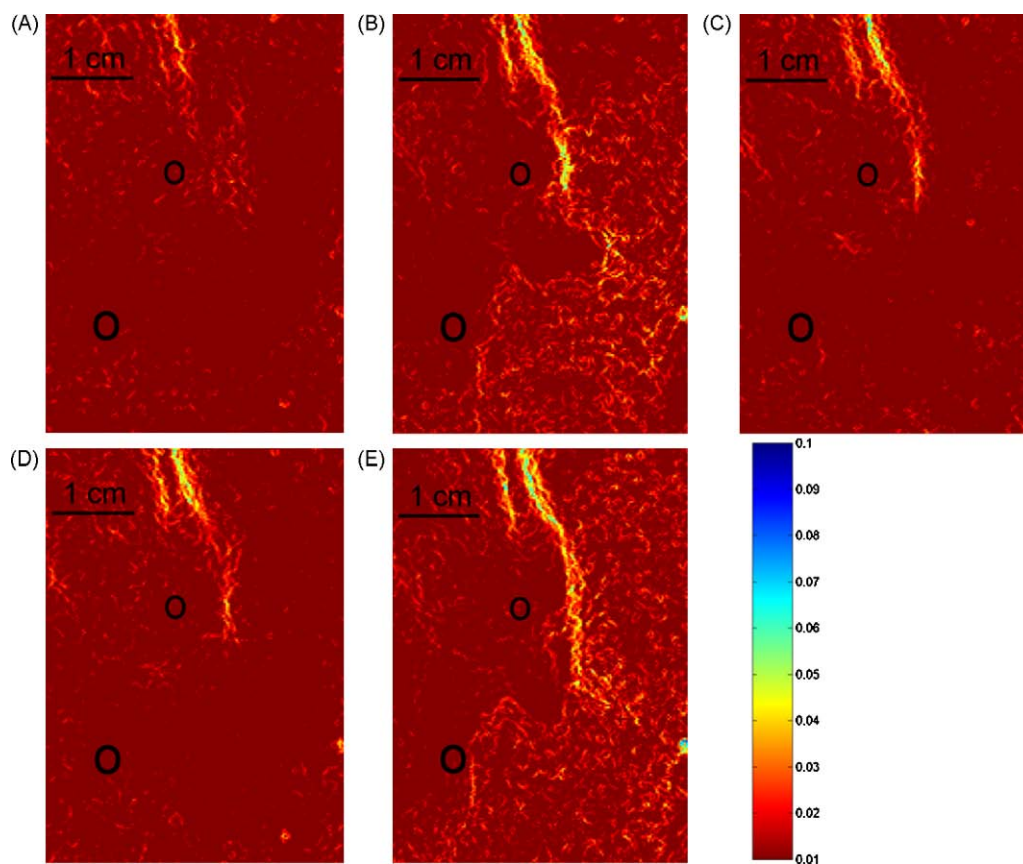


Fig. 4. Images of pH gradients ($[\delta x^2 + \delta y^2]^{1/2}$) in each pixel. Images were captured at: (A) 20:02 day 9, (B) 10:22 day 10, (C) 14:26 day 10, (D) 16:51 day 10 and (E) 10:10 day 11. Black rings were inserted to illustrate end-locations of the bivalves. The color bar denotes pH units per pixel.

cedure. In contrast, this precision was ascribed to only 30–40% of pixels using pre-sample calibration protocols. At the end of experiments (day 17), the spatial precision for 89% of pixels was better than 0.05 pH units using the time-correlated calibration procedure (Fig. 3), while only 24% of pixels were associated with a precision better than 0.05 pH units using the more conventional calibration protocol (Fig. 3A).

Six images were taken before and after the sediment was X-rayed at the end of experiments ($n_{\text{tot}} = 12$; day 17). The temporal precision of measurements was similar for the two sets of images. More than 87% of the pixels were associated with a temporal precision better than 0.05 pH units using the time-correlated calibration (Fig. 3D). For comparison, the precision was better than 0.05 pH units for ~47% of the pixels using conventional calibrations (Fig. 3B). Our study therefore demonstrated and confirmed previous studies by [12] that significantly more pixels in the final pH image were associated with high precision (S.D. < 0.05) when sensor response was evaluated using time-correlated calibrations compared to more conventional pre-calibration protocols. Average S.D. for both the spatial and the temporal precision (overall S.D. < 0.05) were constant using time-correlated (0.01 pH units) and pre-sample (0.03 pH units) calibration procedures, respectively. Using the time-correlated calibration procedure, an additional 46–73% pixels were associated with a precision (S.D.) better than 0.05 pH units.

For future imaging studies the sigmoidal and log-linear approach for time dependent calibrations are highly interesting [8,36]. Also, involvement of nanoparticles or nanostructures for signal enhancement and increased photo-stability provides a performance increasing and drift minimizing tool, recent examples are [37–39].

3.2. Systematic errors or diurnal variations in bivalve activities?

The variation in response for images taken at ~8:00 compared ~20:00 demonstrated differences related to the time of measurement in regions used to evaluate system background (close to the edges of the sensor). The observed time-dependent systematic drift in system response could be a consequence from switching the instrument on and off, affecting the light intensity of the light source and possibly the temperature within the experimental box. Artifacts associated with changes in excitation light intensities are normally cancelled out by the ratiometric procedure [16]. However, time-dependent changes in the spectral properties of the excitation lamp may not be cancelled by the ratiometric procedure. A shift in fluorescence partitioning due to potential fluctuations in temperature would also change the observed sensor response in a methodical way. The quantitative importance of these effects was, however, not individually evaluated. Assuming that this systematic change in pH ($\delta\text{pH}/\delta t$) reflects the maximum “background” contribution from system fluctuations to the measured sensor response, the sensor drift was 0.0025 ± 0.0003 pH units h^{-1} ($n=90$; 5×5 blocks). This systematic drift caused the measured pH to increase during the day and decrease during the night.

To further illustrate and localize small-scale temporal and spatial variations in sensor response, the pH gradient in each pixel was calculated (Fig. 4). The gradients revealed fine structures in the sediment down to single pixel resolution, with an overall structure similar to naturally occurring pore water and distribution patterns created by the bivalves. The latter were at the end of experiment confirmed by the X-radiograph (Fig. 5). In addition to a temporal variability in the systematic error of sensor response, imaging of pH gradients in each pixel suggested time-dependent patterns

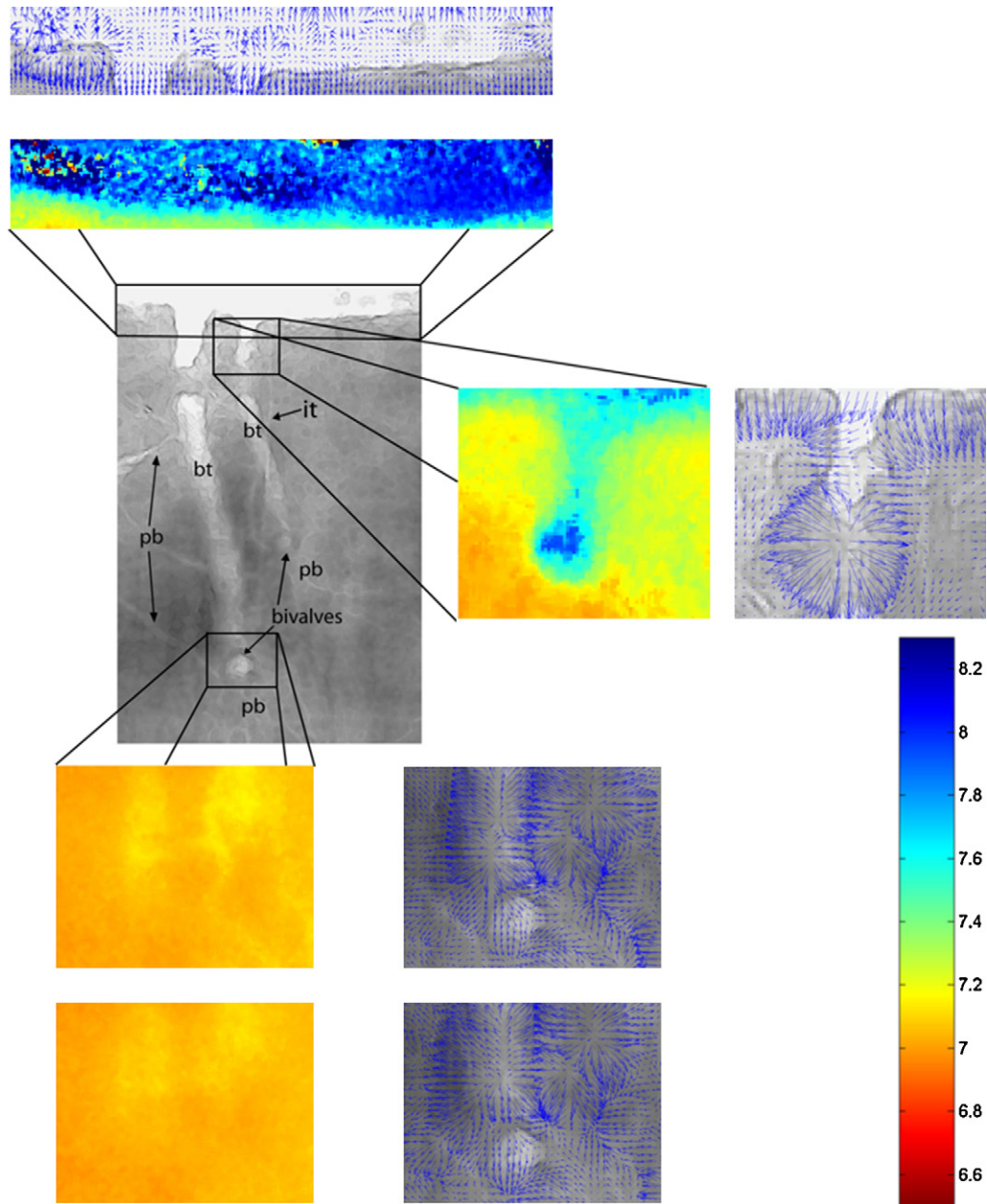


Fig. 5. The large image in the center represents an X-radiograph of the aquarium at the end of the experiment. The final position of the bivalves, their burrowing tracts (bt), inhalent tubes (it), and pedal burrowing tracts (pb) are indicated. *Above radiograph.* A close-up of the sediment surface at the beginning of experiments. *Beside radiograph.* The initial burrowing tract of a bivalve. *Below radiograph.* The sediment surrounding a bivalve just before (upper panels) and after (lower panels) X-rays were taken. Quiver plots (Matlab 6.5) highlight the strong pH gradients associated with imaging of pH distributions in sediments bioturbated by *T. sarsi*.

in activities by the thysirids (Fig. 4). The pH gradients were progressively more developed (magnitude and spatial extension) in all images captured in the morning compared to those obtained in the afternoon and evening.

3.3. General patterns during imaging of pH

The pH imaging sensor qualitatively and quantitatively demonstrated temporal and spatial patterns of pH distributions in the overlying water and sediment matrix during the experiment. Overall, pH of the overlying water was higher than that of the underlying sediment, with a concentration gradient depending on the time of experiment. At the beginning of experiment, there was a distinct drop in pH (from 8.2 to 7.3; Fig. 2C) immediately below the sediment-water interface, likely associated with aerobic min-

eralization of organic material and the re-oxidation of products resulting from anaerobic respiration diffusing from below. While there were regions with more or less constant pH, primarily in deeper sediment layers not initially exposed to macrofaunal reworking, the imaging sensor clearly revealed small and large-scale variations in pH which would normally be obscured by principles of spatial averaging over finite depth intervals (e.g. by pH electrodes). For example, the distinct drop in pH at the sediment surface was associated with gradients of up to 1 pH unit over a distance of less than 5 mm.

The overall pH decrease with time of experiment is likely due to a combined effect from enhanced aerobic organic matter mineralization and induced re-oxidation of reaction products caused by macrofaunal activities, as well as a release of H^+ as a consequence from the reoxidation of symbiotic metabolites. The pH decrease

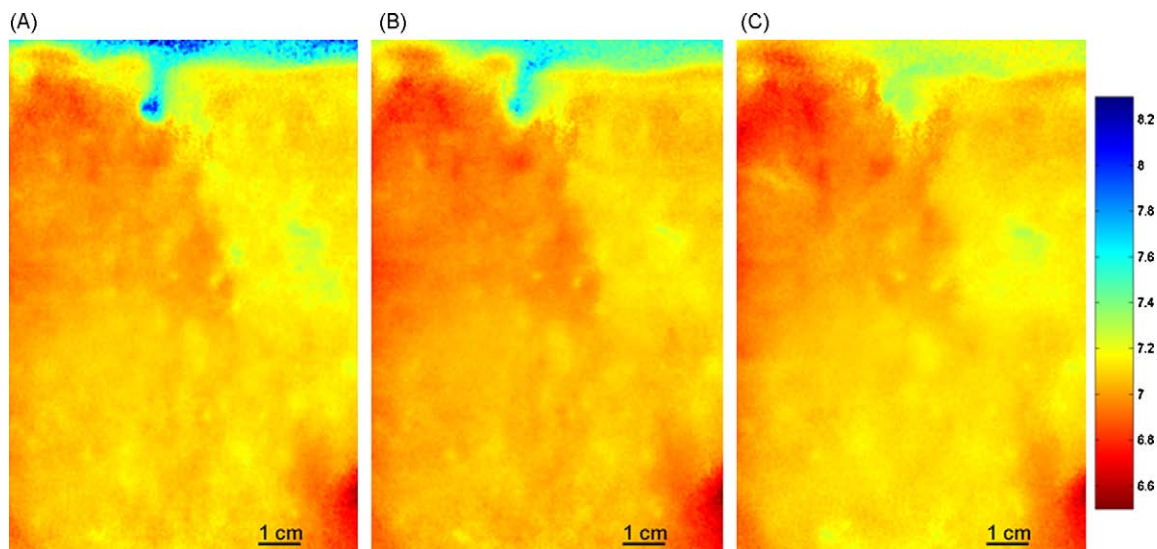


Fig. 6. The images display the acidification of overlying water during the initial period of burrowing by the bivalves. Images of pH are shown after 92 h (A), 100 h (B) and 116 h (C) of experiment. During this period, the pH of the overlying water dropped from >8 to 7.2 despite a continuous flow of seawater to the microcosm. The decrease in pH was likely attributed to pore water irrigation by *T. sarsi* that supplied reduced and acidic compounds through the exhalent tube to the overlying water.

was first observed and was most pronounced in the overlying water (Fig. 6). Initial pH values in the overlying water was consistent with open ocean conditions (~ 8.2), but relatively quickly decreased, reaching a pH of ~ 7 on day 4, and remained more or less constant through day 10. It therefore appeared as the flow of incoming bottom water was insufficient to completely maintain biogeochemical characteristics (i.e. pH) of the overlying water. However, although dissolved oxygen was not directly measured, the frequent visual inspections of the microcosm in general, and the surface sediment in particular, confirmed a well-oxygenated bottom water and sediment surface. Further, considering the alkalinity ($A_T \sim 2350 \mu\text{M}$) and general buffer capacity of the bottom water, the sediment supply of H^+ must have been significant to cause the pH change observed in the overlying water. Preliminary results from follow-up experiments using oxygen and pH electrodes positioned immediately above the opening of the exhalent tube of *T. sarsi* have confirmed a strongly reduced and acidic exhalent stream that may, at least locally, drastically affect pH of bottom waters (data not shown).

On day 17, a tongue of high pH values was observed to extend from the sediment surface into the sediment on the right-hand side of the aquarium close to the region where the inflow of oxygenated bottom water was directed (Figs. 1 and 2D). Although burrowing and irrigation by the thyasirids cannot be completely excluded, the X-ray image integrating faunal activities does not support extensive and large-scale bioturbation patterns directly associated with this progressive evolution of pH (Fig. 5). Alternatively, extensive and more long-term reworking of particles by the highly extensible foot of this small bivalve may have contributed to a partial disruption of the sediment structure and thereby increased the permeability of the sieved sediment. As an indirect consequence from *T. sarsi* bioturbation activities by the extensible foot, overlying water could progressively passively penetrate relatively deep into the sediment immediately below the tube that supplied oxygenated replacement water.

3.4. Changes in pH due to activities by *T. sarsi*

With time, the bivalves created burrows around which pH changed dramatically compared to the adjacent sediment (Fig. 5 and 6A). From visual observations, the bivalves had burrowed

into the sediment ~ 3 h after their introduction into the aquarium. About 16 h after the addition of animals (i.e. the following morning) there was clear evidence of a burrowing tract (Figs. 5 and 6A). This cavity is the beginning of a pathway from the sediment surface to the final position of the bivalve in the sediment, with the remainder of the tract being consecutively refilled with sediment. This tract should be of no use to the burrowed animal, as it is known to construct an inhalent tube with its foot for ventilation purposes and for direct contact with the overlying water.

The pH within the burrowing tract at the beginning of the experiment was >8.0 , i.e. significantly higher than that of the surrounding sediment (pH 7.0–7.5) and more similar to the pH of the overlying water (Figs. 5 and 6A). Later in the experiment, when the burrowing tracts were refilled, the pH within them was lower than the surrounding sediment (6.90 compared to 7.05; Fig. 2D). Lower pH values in relict formations confirm observations by Zhu et al. [25]. These authors reported increased concentrations of CO_2 in relict burrow structures by the polychaete *Nephtys incisa*, a consequence suggested related to the local injection of reactive substrate (e.g. mucus) and energetically favorable oxidants (Mn- and Fe-oxides) formed within the burrow walls. Alternatively, the burrowing tracts may in our study have constituted pathways for the bivalve to eject water of low pH (including symbiotic metabolites) to the overlying water. In addition to lower pH measured in the relict burrow, the latter assumption was strongly supported by the drastic pH decrease in the overlying water after addition of the bivalves (Fig. 6). Significant pH gradients close to the burrows of *T. sarsi* were confirmed by Quiver plots (Matlab 6.5). The strongest gradients were observed immediately adjacent to the burrowing tracts, inhalent tube and pedal tracts (Fig. 5). For example, during the initial burrowing of one of the bivalves, gradients of up to 1.16 pH units per mm (0.32 units per pixel) were observed (burrowing tract in Fig. 6A). In contrast to the lower pH in burrowing tracts, pedal tracts demonstrated higher pH than the surrounding sediment (Fig. 2D). Interestingly, at the end of experiments the narrow pedal tracts seemed to be directed towards the region where inflow of overlying water likely penetrated the sediment (Fig. 2D). This pattern may indicate an intentional pathway whereby the bivalve could actively reach oxygenated bottom water, possibly containing soluble sulfides (e.g. thiosulfate and acid volatile sulfides) in addition to other oxidants such as nitrate.

4. Conclusions

Utilizing time-correlated pixel-by-pixel calibration protocols during imaging, close to 90% of the pixels were associated with a precision (S.D.) of <0.05 pH units at the end of an experimental period of 17 days. Average S.D. for both the spatial and the temporal precision (overall S.D. <0.05) were constant using time-correlated (0.01 pH units) and pre-sample (0.03 pH units) calibration procedures, respectively. Using the time-correlated calibration procedure, an additional 46–73% of pixels were associated with a precision (S.D.) better than 0.05 pH units. Strong pH gradients were demonstrated not only across the sediment-water interface but also associated with bioturbation activities immediately adjacent to *T. sarsi* burrowing tracts, inhalant tubes and pedal tracts in the sediment matrix. Gradients of up to 1.16 pH units per mm were observed.

Acknowledgements

Financial support was obtained by the Swedish Research Council (VR), the Foundation for Strategic Environmental Research (MISTRA), the Swedish Research Council for Environment, Agricultural Sciences and Spatial Planning (FORMAS), the Royal Swedish Academy of Sciences, and the Swedish Marine Research Centre (GMF). E. Väänänen provided technical support. R. Rosenberg and K. Norling assisted during field sampling.

References

- [1] R.N. Glud, N.B. Ramsing, J.K. Gundersen, I. Klimant, *Marine Ecology-Progress Series* 140 (1996) 217–226.
- [2] N. Stromberg, *Environmental Science & Technology* 42 (2008) 1630–1637.
- [3] S. Hulth, R.C. Aller, P. Engstrom, E. Selander, *Limnology and Oceanography* 47 (2002) 212–220.
- [4] Q.Z. Zhu, R.C. Aller, Y.Z. Fan, *Environmental Science & Technology* 39 (2005) 8906–8911.
- [5] J.I. Peterson, S.R. Goldstein, R.V. Fitzgerald, D.K. Buckhold, *Analytical Chemistry* 52 (1980) 864–869.
- [6] N. Stromberg, E. Mattsson, A. Hakonen, *Analytica Chimica Acta* 636 (2009) 89–94.
- [7] C. McDonagh, C.S. Burke, B.D. MacCraith, *Chemical Reviews* 108 (2008) 400–422.
- [8] A. Hakonen, S. Hulth, *Analytica Chimica Acta* 606 (2008) 63–71.
- [9] P.C.A. Jeronimo, A.N. Araujo, M. Montenegro, *Talanta* 72 (2007) 13–27.
- [10] D.A. Nivens, M.V. Schiza, S.M. Angel, *Talanta* 58 (2002) 543–550.
- [11] D. Wencel, B.D. MacCraith, C. McDonagh, *Sensors and Actuators B-Chemical* 139 (2009) 208–213.
- [12] N. Stromberg, S. Hulth, *Analytica Chimica Acta* 550 (2005) 61–68.
- [13] R.B. Thompson, J.R. Lakowicz, *Analytical Chemistry* 65 (1993) 853–856.
- [14] R.Y. Tsien, M. Poenie, *Trends In Biochemical Sciences* 11 (1986) 450–455.
- [15] H. Hochreiner, I. Sanchez-Barragan, J.M. Costa-Fernandez, A. Sanz-Medel, *Talanta* 66 (2005) 611–618.
- [16] Z. Zhujun, W.R. Seitz, *Analytica Chimica Acta* 160 (1984) 47–55.
- [17] N. Stromberg, S. Hulth, *Sensors and Actuators B-Chemical* 90 (2003) 308–318.
- [18] H. Stahl, A. Glud, C.R. Schroder, I. Klimant, A. Tengberg, R.N. Glud, *Limnology and Oceanography-Methods* 4 (2006) 336–345.
- [19] N. Stromberg, S. Hulth, *Sensors and Actuators B-Chemical* 115 (2006) 263–269.
- [20] R.J. Diaz, R. Rosenberg, *Science* 321 (2008) 926–929.
- [21] R. Vaquer-Sunyer, C.M. Duarte, *Proceedings of the National Academy of Sciences of the United States of America* 105 (2008) 15452–15457.
- [22] S.C. Dufour, H. Felbeck, *Marine Ecology-Progress Series* 320 (2006) 185–194.
- [23] P.R. Dando, A.J. Southward, E.C. Southward, *Marine Ecology-Progress Series* 280 (2004) 181–187.
- [24] S.C. Dufour, H. Felbeck, *Nature* 426 (2003) 65–67.
- [25] Q.Z. Zhu, R.C. Aller, Y.Z. Fan, *Marine Chemistry* 101 (2006) 40–53.
- [26] S. Hulth, R.C. Aller, F. Gilbert, *Geochimica Et Cosmochimica Acta* 63 (1999) 49–66.
- [27] K. Soetaert, A.F. Hofmann, J.J. Middelburg, F.J.R. Meysman, J. Greenwood, *Marine Chemistry* 106 (2007) 380–401.
- [28] K. Caldeira, M.E. Wickett, *Nature* 425 (2003) 365–366.
- [29] S. Widdicombe, S.L. Dashfield, C.L. McNeill, H.R. Needham, A. Beesley, A. McEvoy, S. Oxnevad, K.R. Clarke, J.A. Berge, *Marine Ecology-Progress Series* 379 (2009) 59–75.
- [30] Q.Z. Zhu, R.C. Aller, Y.Z. Fan, *Geochimica Et Cosmochimica Acta* 70 (2006) 4933–4949.
- [31] L. Arneborg, *Continental Shelf Research* 24 (2004) 443–460.
- [32] O. Lindahl, A. Belgrano, L. Davidsson, B. Hernroth, *Ices Journal of Marine Science* 55 (1998) 723–729.
- [33] P. Engstrom, T. Dalsgaard, S. Hulth, R.C. Aller, *Geochimica Et Cosmochimica Acta* 69 (2005) 2057–2065.
- [34] A. Jang, J.H. Lee, P.R. Bhadri, S.A. Kumar, W. Timmons, F.R. Beyette, I. Papautsky, P.L. Bishop, *Environmental Science & Technology* 39 (2005) 6191–6197.
- [35] I. Hansson, *Deep-Sea Research* 20 (1973) 479–491.
- [36] A. Hakonen, S. Hulth, *Talanta* 80 (2010) 1964–1969.
- [37] C. Maule, H. Gonçalves, C. Mendonça, P. Sampaio, J.C.G. Esteves da Silva and P. Jorge, *Talanta* 80, 1932–1938.
- [38] C. McDonagh, O. Stranik, R. Nooney, B.D. MacCraith, *Nanomedicine* 4 (2009) 645–656.
- [39] A. Hakonen, *Analytical Chemistry* 81 (2009) 4555–4559.